Supporting Information

Benedetti et al. 10.1073/pnas.1713845115

SI Materials and Methods

Plasmids. Expression vectors encoding nMagHigh1-EGFP-CAAX, pMagFast2(3x)-iRFP, and iSH2-pMag(3x)-iRFP were kind gifts from Moritoshi Sato, University of Tokyo, Tokyo. Vectors encoding the photolyase homology region domain (Cry2PHR, amino acids 1–498) of *A. thaliana* Cryptochrome 2 (Cry2) fused to mCherry (mCherry-Cry2), and the N-terminal region of CIB1 (CIBN; amino acids 1–170) fused to GFP and containing a C-terminal CAAX box (CIBN-GFP-CAAX) were kind gifts from Chandra Tucker, University of Colorado, Denver. The following vectors were obtained from Addgene: pLL7.0:Venus-iLID-Mito (from ActA) (plasmid 60413), pLL7.0:Venus-iLID-CAAX (from KRas4B) (plasmid 60411), pLL7.0:tgRFPt-SspB Wt (Nano variant) (plasmid 60415), and pLL7.0:tgRFPt-SspB R73Q (Micro variant) (plasmid 60416). ER-nMag, ER-iLID, ER-CIBN, Mito-nMag(2x), Rab5-nMag, PM-nMag(3x), and mCherry-pMagFast2(3x)-MTMR1 [*Homo sapiens* myotubularin 1 (MTMR1) NCBI reference sequence: XM_011531173.2] were designed and generated in collaboration with VectorBuilder (Cyagen Biosciences) and are described in Tables S1 and S2. To generate the pMagFast2(3x)-mCherry and pMagFast2(3x)-tgRFPt vectors, mCherry and tgRFPt coding sequences were PCR-amplified from the mCherry-Cry2 and tgRFPt-SspB plasmids, respectively, and cloned into pMagFast2(3x)-iRFP using KpnI and XbaI sites. Mito-nMag(1x) was generated through the PCR amplification of the nMagHigh1-EGFP coding sequence from nMagHigh1-EGFP-CAAX and inserted into a pGFP-OMP25 vector (P.D.C. laboratory, unpublished) cut with NheI and XhoI sites. CIBN-EGFP-Mito was generated by PCR-amplifying the CIBN coding sequence from CIBN-GFP-CAAX and cloned into pGFP-OMP25 at NheI and AgeI cloning sites. pLL7.0:Venus-iLIDV416T-Mito, Venus-iLIDI427T-Mito, ER-iLIDV416T, and ER-iLIDI427T were generated by site-directed mutagenesis (QuikChange II XL; Agilent technologies) with the following primers: 5′-agtctcggatcagtaatcgtgaaatttttctcgatccgttccagt-3′ and 5′-actggaacggatcgagaaaaatttc-**acg**attactgatccgagact-3′ for the V416T variant and 3′-ggaatcgctcgcaaaaatcgttgggttgtcaggcagtc-3′ and 5′-gactgcctgacaaccca**acg**attttgcgagcgattcc-3′ for the I427T variant. Lys-nMag was assembled by fusing the PCR-amplified lysosomal targeting sequence of p18 (Ragulator complex protein of LAMTOR1, NCBI reference sequence: NP_060377.1) to the Tom70-nMagHigh1-EGFP vector at EcoRI and BamHI sites. This Tom70-nMagHigh1-EGFP vector was generated by inserting the nMagHigh-EGFP sequence in pEYFP-MitoTrap (Addgene plasmid 46942) at BamHI and HpaI sites. Lamp1-iRFP was generated by PCR-amplifying the *H. sapiens* lysosomal associated membrane protein 1 (LAMP1) coding sequence (NCBI reference sequence: NM_005561.3) synthetized as a gBlocks Gene Fragment (Integrated DNA Technologies), which was inserted at EcoRI and BamHI sites of piRFP670-N1 (Addgene plasmid 45457). The plasmid iRFP-FYVE was generated by replacing the EGFP coding sequence from EGFP-FYVE, a kind gift from Harald Stenmark, Oslo University Hospital, Oslo, with a iRFP670 coding sequence amplified from piRFP670-N1 (Addgene plasmid 45457) and inserted at NheI and XhoI sites. The mCherry-pMagFast2(3x)-5ptase$_{OCRL}$ was synthetized by digesting mCherry-Cry2-5ptase$_{OCRL}$ (1) with NotI and PvuI, and then ligated to pMagFast2(3x) amplified from pMagFast2(3x)-iRFP. mCherry-SspB was generated by cutting mCherry-pMagFast2(3x)-5ptase$_{OCRL}$ with NotI and BamHI, and then inserting the SspB coding sequence after it was PCR-amplified from tgRFPt-SspB Wt. The resulting plasmid was used to generate the mCherry-SspB R73Q variant by site-directed mutagenesis (QuikChange II XL; Agilent technologies). mCherry-SspB R73Q-5ptase$_{OCRL}$ was cloned by digesting mCherry-pMagFast2(3x)-5ptase$_{OCRL}$ with NheI and PvuI and inserting the mCherry-SspB R73Q coding sequence amplified from mCherry-SspB R73Q vector. For all of these clones, PCR amplification of the fragments and subsequent ligation was performed using the In-Fusion Cloning Kit and online tools (BD Clontech, Takara Bio). The mCherry-Cry2-5ptase$_{OCRL}$ and iRFP-PH$_{PLC\delta}$ plasmids were previously described (1). All plasmids were verified by sequencing (Genewiz).

Cell Culture. HeLa M, COS7, and human dermal fibroblasts were cultured at 37 °C and 5% CO_2 in DMEM (Life Technologies) which was supplemented with 10% FBS (Life Technologies), 1 mM sodium pyruvate (Life Technologies), 100 U/mL penicillin, 100 μg/mL streptomycin (Life Technologies), MEM-Non-Essential Amino Acids (Life Technologies), and 1 mM L-glutamine (Life Technologies). All lines were tested monthly and verified as being mycoplasma-free (MycoSensor PCR Assay Kit; Agilent Technologies).

Neuronal Culture. Primary cultures of hippocampal and cortical neurons were generated from mouse brains. Cortex or hippocampi of postnatal day 0–2 pups were dissected in cold HBSS 1× supplemented with 10 mM Hepes, pH 7.4, 100 U/mL penicillin, 100 μg/mL streptomycin, and 1 mM sodium pyruvate (all reagents from Life Technologies)]. Cells of these tissues were then dissociated by papain treatment [20 U/mL papain (Worthington Biochemical corporation) and 0.2 mg/mL L-cysteine (Sigma) in HBSS, pH 7.4] at 37 °C for 15 min and trituration. Live, dissociated cells (Trypan Blue exclusion) were counted and seeded in plating medium [Neurobasal supplemented with 5% FBS, 1% Glutamax, and 2% B27 (all reagents from Life Technologies)] at 3.4×10^4 cells per cm^2 on poly-D-lysine-coated (Sigma), glass-bottomed Petri dishes (MatTek corporation). Three hours after transfection the serum-based medium was replaced with serum-free neuronal medium and cells were maintained in vitro at 37 °C and 5% CO_2. Transient transfection was performed between 4–14 d in vitro (DIV). All experimental procedures involving the use of mice were performed in agreement with the Yale University Institutional Animal Care and Use Committee.

Transient Transfection and Live-Cell Imaging. For live-cell imaging experiments cells were seeded on glass-bottomed dishes (MatTek Corp.) coated with 0.005 mg/mL human plasma fibronectin (EMD Millipore) at 37 °C for 30 min and then washed three times with sterile water. Fibroblastic cells were seeded at a concentration of $10–15 \times 10^4$ cells per cm^2 per dish and transfected after 24 h with Lipofectamine 2000 (Life Technologies), following the manufacturer's instructions. To study prey-protein recruitment at the ER cells were transfected with cDNAs encoding ER-nMag(2x) (bait) and pMagFast2-tgRFPt (prey) at a 2:1 ratio, ER-iLID (bait) and tgRFPt-SspB (prey) at a 1:1 ratio, or ER-CIBN (bait) and Cry2-mCherry (prey) at a 2:1 ratio, in OptiMEM-I (Thermo Fisher Scientific) (1:4 DNA:lipofectamine ratio). For the mitochondrial targeting of prey protein cells were transfected with cDNAs encoding the following pairs: Mito-nMag(2x) (bait) and pMagFast2(3x)-mCherry (prey) at a 2:1 ratio, iLID-Mito (bait) and mCherry-SspB (prey) at a 1:1 ratio, CIBN-Mito (bait) and Cry2-mCherry (prey) at a 2:1 ratio, or Mito-nMag(1x) (bait) and pMagFast2(3x)-mCherry (prey) at a 2:1 ratio, with 1.5 μg total DNA per dish (1:4 DNA: lipofectamine ratio). For the experiments recruiting prey to a single lysosome HeLa cells were cotransfected with Lys-nMag (bait), pMagFast2(3x)-tgRFPt (prey), and Lamp1-iRFP (reporter) at a

3:2:1 ratio, with 2 μg total DNA (1:2 DNA:lipofectamine ratio). For the experiments recruiting prey to a single endosome HeLa cells were cotransfected with Rab5-nMag (bait), pMagFast2(3x)-mCherry (prey), and iRFP-FYVE (reporter) at a 3:2:1 ratio, with 2 μg total DNA (1:2 DNA: lipofectamine ratio) or Rab5-nMag (bait), mCherry-pMagFast2(3x)-MTM1 (prey), and iRFP-FYVE (reporter) at a 2:1:1 ratio, with 2 μg total DNA (1:2 DNA: lipofectamine ratio). The direct comparison between Cry2/CIB1, iLID, and Magnets systems in PI(4,5)P_2 modulation was performed in COS7 cells transfected with CIBN-GFP-CAAX (bait), mCherry-Cry2-5ptaseOCRL (prey), and iRFP-$PH_{PLC\delta}$ (reporter) at a 2:3:1 ratio or pLL7.0:Venus-iLID-CAAX (bait) mCherry-SspBR73Q-5ptaseOCRL (prey), and iRFP-$PH_{PLC\delta}$ (reporter) at a 2:2:1 ratio or PM-nMag(1x) (bait), mCherry-pMagFast2(3x)-$5ptase_{OCRL}$ (prey), and iRFP-$PH_{PLC\delta}$ (reporter) at a 3:2:1 ratio, with 2 μg total DNA. Rapid modulation of PI(4,5)P_2 at the plasma membrane was performed in HeLa cells that were cotransfected with vectors encoding PM-nMag(3x) (bait), mCherry-pMagFast2(3x)-$5ptase_{OCRL}$ (prey), and iRFP-$PH_{PLC\delta}$ (reporter) at a 3:2:1 ratio, with 2 μg total DNA (1:2 DNA:lipofectamine ratio). Cells were incubated with the transfection mix for 2–4 h. Subsequently, the serum-free medium was replaced by complete DMEM and cells were incubated at 37 °C. Cells expressing Magnets vectors were incubated at 28 °C for 6–10 h and before imaging cells were incubated at 37 °C for at least 1 h. All imaging experiments were performed at 37 °C in live-cell imaging solution (Life Technologies). Single-lysosome prey recruitment was performed in 9 DIV cortical neurons transfected with Lys-nMag (bait), pMagFast2(3x)-tgRFPt (prey), and Lamp1-iRFP (reporter) at a 3:2:1 ratio, with 1.5 μg total DNA (1:4 DNA:lipofectamine ratio). Plasma membrane modulation of PI(4,5)P_2 was tested in 10–12 DIV hippocampal neurons transfected with PM-nMag(3x) (bait), mCherry-pMagFast2(3x)-$5ptase_{OCRL}$ (prey), and iRFP-$PH_{PLC\delta}$ (reporter) at a 3:2:1 ratio, with 1.5 μg total DNA (1:4 DNA: lipofectamine ratio).

Confocal Microscopy. Spinning-disk confocal microscopy was performed using the Improvision UltraVIEW VoX system (PerkinElmer) built around a Nikon Ti-E inverted microscope and controlled by Volocity software (Improvision). Imaging was performed at 37 °C with a 63× PlanApo oil objective (1.45 N.A.). To prevent unwanted photoactivation of the optogenetic dimerizers, transfected cells were identified with the fluorescence emitted by different red fluorescent tags using a bandpass excitation filter ET 560/30. A 488-nm laser was used to excite EGFP, a 561-nm laser for mCherry and tgRFPt, and a 640-nm laser for iRFP670. The fluorescence emitted was detected with 527/55-nm, 615/70-nm, and 705/90-nm filters, respectively. Whole-cell activation of the photo switches was achieved by irradiating the field of view with 488-nm laser pulses of 100–200 ms (3×10^{-3} W/cm^2). A built-in photo-perturbation unit was used to deliver 488-nm light (7.07 W/cm^2) pulses with subcellular precision.

Image Analysis and Statistics. Association and dissociation rates for each dimerization system were calculated from changes in prey fluorescence inside a cytosolic ROI before, during, and after the photoactivation recruiting the prey to mitochondrial membranes. The change in average fluorescence inside of this ROI was calculated using the software Fiji (ImageJ 1.48k, fiji.sc/wiki/index.php/Fiji), and the remainder of the quantification was carried out in Python. The change in fluorescence was calculated as $\frac{\Delta f}{f_*} = \frac{f[t_i] - f[t_*]}{f[t_*]}$, where $f[t] = (F_{ROI}[t] - F_{bkg}[t]) / (F_{cell}[t] - F_{bkg}[t])$, where F_{ROI} is the mean fluorescence measured in the cytosolic ROI, F_{bkg} is the mean fluorescence intensity measured in an area of the background, F_{cell} is the mean fluorescence measured in the whole cell to normalize for photobleaching, and t_i denotes the point in time. The fluorescence changes associated to the plasma membrane [empty prey or mCherry-pMagFast2(3x)-$5ptase_{OCRL}$ and iRFP-$PH_{PLC\delta}$] or at mitochondria were calculated with the same equation but, in this case, the ROI for each time point was identified by generating a binary mask using the fluorescence signal associated with the plasma membrane or with the mitochondrial bait, respectively. Prey and iRFP-FYVE changes at endosomes were calculated by measuring fluorescence variations in manually drawn ROIs around each endosome of interest. Statistical analyses were carried out in GraphPad Prism 7 (GraphPad Software).

System Kinetics. The kinetics of these optogenetic systems cannot simply be modeled with two compartments undergoing exchange, primarily due to noninstantaneous activation/deactivation. We employed a model-agnostic approach to determine a characteristic on and off rate for each optogenetic system. To this aim, we calculated the total change in normalized fluorescence of the cytosol due to the system response to the activation laser as $\Delta S = \langle S(t) \rangle_{0 \le t \le t_o} - \langle S(t) \rangle_{tmin}$, where $S = \frac{\Delta f}{f_*}$, t_o is the time when the activation laser was turned on, t_1 is the time when the activation laser was turned off, and tmin are the 20 time points where S(t) is the smallest. We then found the half-lives $\tau_{1/2}^{ON}$, the time before t_1 that minimizes $S(t) - 0.5\Delta S$, and $\tau_{1/2}^{OFF}$, the time after t_1 that minimizes the same quantity. Since several $\tau_{1/2}^{ON}$ times were smaller than the sampling time of these experiments we interpolated linearly between time points, sampling at an interval of ∼2 ms. We also examined protein recruitment to mitochondria by examining the fluorescence of the mitochondrial volume itself within 30 s of when the system was activated throughout the entire cell with blue-light pulses of 0.5 Hz. Here, we determined the amplitude of the system response as $\Delta S = \langle S(t) \rangle_{t_{max}-20 \le t \le t_{max}} - S(t = t_o)$, where t_{max} is the last time point in the series, and then calculated the recruitment half-time, $\tau_{1/2}^{REC}$, by finding the time that minimized $S(t) - 0.5\Delta S$. The uncertainty in $\tau_{1/2}^{ON}$, $\tau_{1/2}^{OFF}$, and $\tau_{1/2}^{REC}$ are straightforward to estimate using the variance in fluorescence at each time point and the equation for a line. Since the interpolation is linear, the only error relevant to each $\tau_{1/2}$ is the error in the fluorescence at the time-points on either side of it. The line from the preceding data point, (t_o, y_o), to the first point after the $y_{0.5} = 0.5\Delta S$ threshold has been crossed, (t_1, y_1), has an uncertainty in its slope given by $\delta m = |m \frac{\sqrt{\delta y_1^2 + \delta y_o^2}}{y_1 - y_o}|$, where we are assuming, that there is no uncertainty in t. The line connecting (t_o, y_o) to $(t_{1/2}, y_{1/2})$ can be rearranged to solve for $t_{1/2}$ as $t_{1/2} = \frac{y_{1/2} - y_o}{m} + t_o$, which yields an uncertainty of the crossing time of $\delta t_{1/2} = |\frac{y}{m}| \sqrt{\left(\frac{\delta y}{y}\right)^2 + \left(\frac{\delta m}{m}\right)^2}$, where $y = y_{1/2} - y_o$ and $\delta y = \sqrt{\delta y_{1/2}^2 + \delta y_o^2}$.

Quantitative Analysis of the Spatial Confinement of Protein Dimerization. HeLa cells expressing ER-CIBN (bait) and Cry2-mCherry (prey) at a 2:1 ratio, ER-iLID (bait) and tgRFPt-SspB (prey) at a 1:1 ratio, and ER-nMag(2x) (bait) and pMagFast2(3x)-tgRFPt (prey) at a 2:1 ratio were irradiated in an illumination ROI of 3 μm × 10 μm (x–y dimension) with 488-nm light (7.07 W/cm2) pulses of 200 ms with a frequency of 0.5 Hz for 5 min. The extent of prey–bait dimer formation at the ER after 1 and 5 min of light excitation was quantified as the ratio between the area of dimerization and the area of photoexcitation (3 μm × 10 μm), where the dimerization area was visually identified and selected with a manually drawn ROI, with the software Fiji.

To quantify the distance of protein dimerization outside of the illumination ROI, and provide a more systematic quantification of the spatial distribution of dimers in time, we examined the fluorescence within an Intensity ROI ($ROI_{Intensity}$, 60 pixels

wide, 125 pixels long), which was converted to units of basal fluorescence by normalizing by an intracellular ROI (ROI_{Basal}) that was drawn away from the illumination area. Additionally, to account for background and camera offset, an extracellular ROI was also drawn ($ROI_{Background}$; see Fig. S7*A* for illustrations of all ROIs). The intensity inside of these ROIs was used to calculate the fluorescence at a given displacement from the edge of the illumination ROI, at each point in time, as $f[d,t] = \frac{\langle ROI_I[d,t]\rangle_s - M[ROI_{out}]}{M[ROI_{basal}] - M[ROI_{out}]}$, where $\langle ROI_I[d,t]\rangle_s$ denotes an average taken along the short axis of the intensity ROI, and M[ROI] is the median intensity inside of a given ROI. This normalized intensity, a function of both time and displacement from the edge of the illumination region, was arranged in a 2D array, which was then averaged with the other time-series for each system. The medians and intensity averaging within various ROIs were done using the PYthon Microscopy Environment. We defined the spread distance from ROI as the farthest positive distance from the edge of the illumination ROI at which f is 2 or larger (Fig. S7*B*). This denotes the distance at which spread has occurred substantially enough that the prey fluorescence has doubled over the prey fluorescence within the inactivated, intracellular ROI, ROI_{Basal}.

1. Idevall-Hagren O, Dickson EJ, Hille B, Toomre DK, De Camilli P (2012) Optogenetic control of phosphoinositide metabolism. *Proc Natl Acad Sci USA* 109:E2316–E2323.

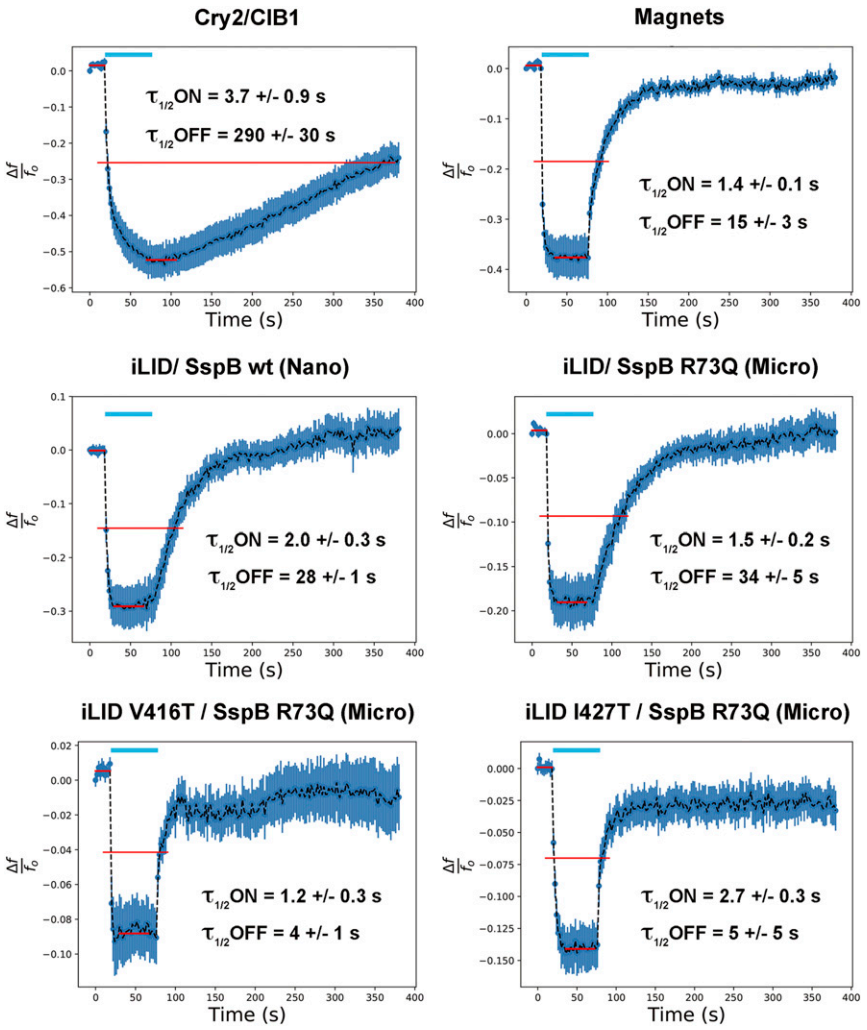

Fig. S1. Analysis of association and dissociation kinetics of optical dimerization systems in living cells. Kinetics of dimer formation and dissociation for each optogenetic pair estimated by measuring the rate of cytosolic fluorescence redistribution in primary human fibroblasts transfected with a mitochondrial bait and an mCherry-tagged soluble prey [n = 23 Cry2/CIB1 (CRY2PHR/CIBN), 20 Magnets (nMagHigh(2x)/pMagFast2(3x)), 27 iLID/SspB wt (Nano), 22 iLID/SspB R73Q (Micro), 26 iLIDV416T/SspB R73Q (Micro), and 23 iLIDI427T/SspB R73Q (Micro); three independent experiments]. Protein dimerization was induced by irradiating the entire cell with blue-light pulses (200 ms at 0.5 Hz, 3×10^{-3} W/cm^2) for 1 min. Images of the prey were acquired with a frame rate of 0.5 Hz, and the mCherry fluorescence in a region of cytoplasm not including mitochondria was plotted. On kinetics are similar, while off kinetics vary more substantially. The calculated values have been summarized in Table S3.

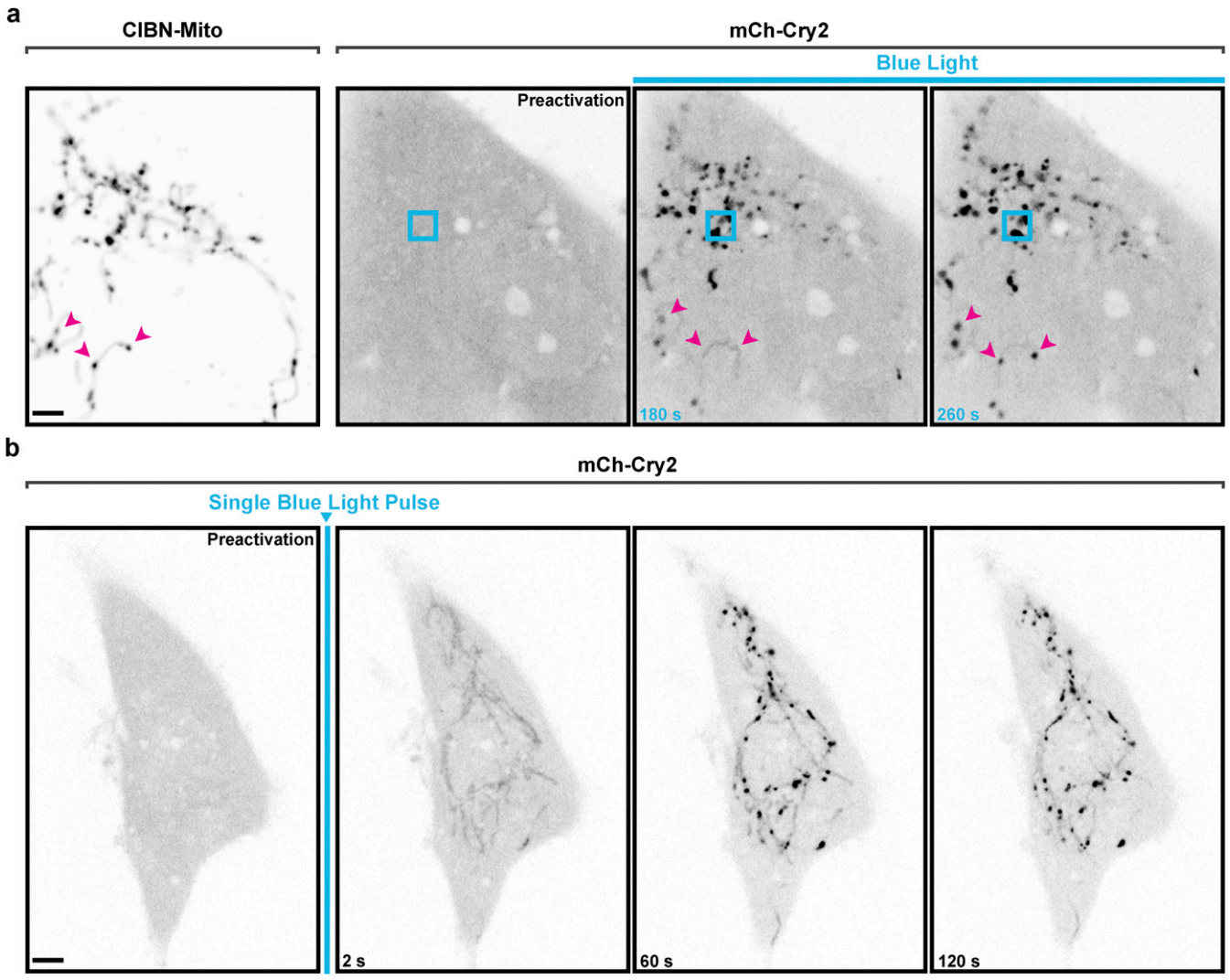

Fig. S2. The enrichment of activated Cry2 on the surface of intracellular organelles is followed by its homooligomerization. (*A*) Human fibroblast cotransfected with the mitochondrial bait CIBN-Mito and the soluble prey mCherry-Cry2. Prolonged pulsed illumination of the soluble Cry2 fusion protein in a 3-μm × 3-μm area (blue box) results in the progressive association of the photoswitch to its binding partner CIBN on target organelles (mitochondria). The three sequential images show the progressive clustering of photoactivated Cry2 and its binding to mitochondria (small arrows), including those outside of the irradiation area (see also Movie S3). This clustering of Cry2 is accompanied by clustering of its membrane-tethered binding partner (CIBN-Mito) as shown by the micrograph at the left, which was taken at the end of the illumination period. (Scale bar: 3 μm.) (*B*) The clustering of Cry2 is not dependent on the area of photoexcitation. Oligomerization also occurs when the entire cell is illuminated with a single 488-nm pulse of 200 ms (Movie S4). (Scale bar: 5 μm.)

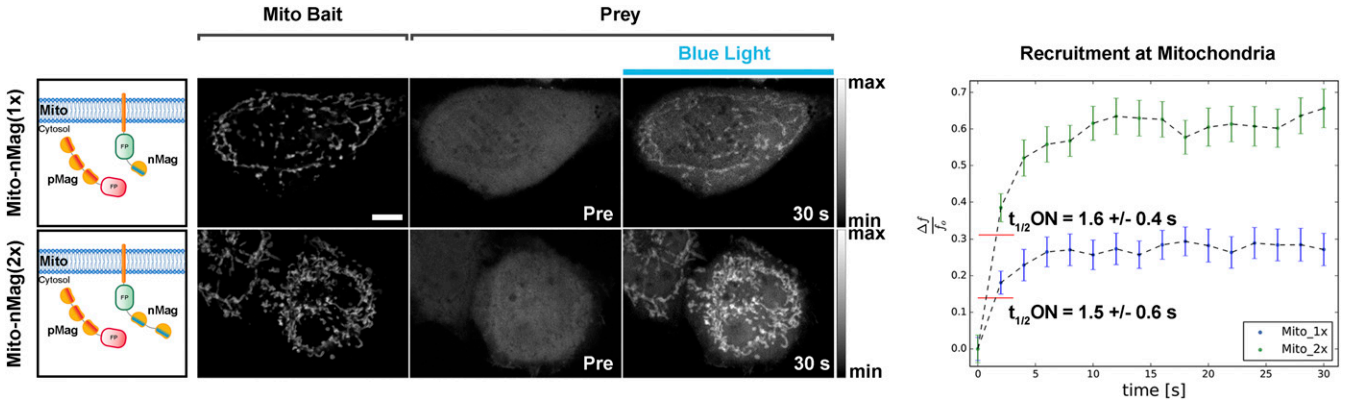

Fig. S3. The use of high-avidity baits increases the local capture of prey protein without a major effect on the association kinetics. HeLa cells expressing the mitochondrial baits Mito-nMag(1x) or Mito-nMag(2x) and the soluble prey pMagFast2(3x)-mCherry before and after blue-light excitation. (Scale bar: 10 μm.) As demonstrated by the plots (*Right*), the amount of prey recruited to mitochondria is substantially higher (around two times) ($P < 0.0001$) in cells expressing the bait containing two negative Magnets than in cells expressing the bait containing only one Magnet. This difference is not associated with a relevant alteration in the switch-on kinetic of the system [$\tau_{1/2}^{ON} = 1.5 \pm 0.6$ s for Mito-nMag(1x) and 1.6 s $\pm$ 0.4 s for Mito-nMag(2x)]. Fluorescence redistribution was measured in 25 cells expressing Mito-nMag(1x) and 31 Mito-nMag(2x) collected in three independent experimental sessions. Data were statistically analyzed with a two-way ANOVA followed by Sidak's multiple comparison test, with the software GraphPad Prism.

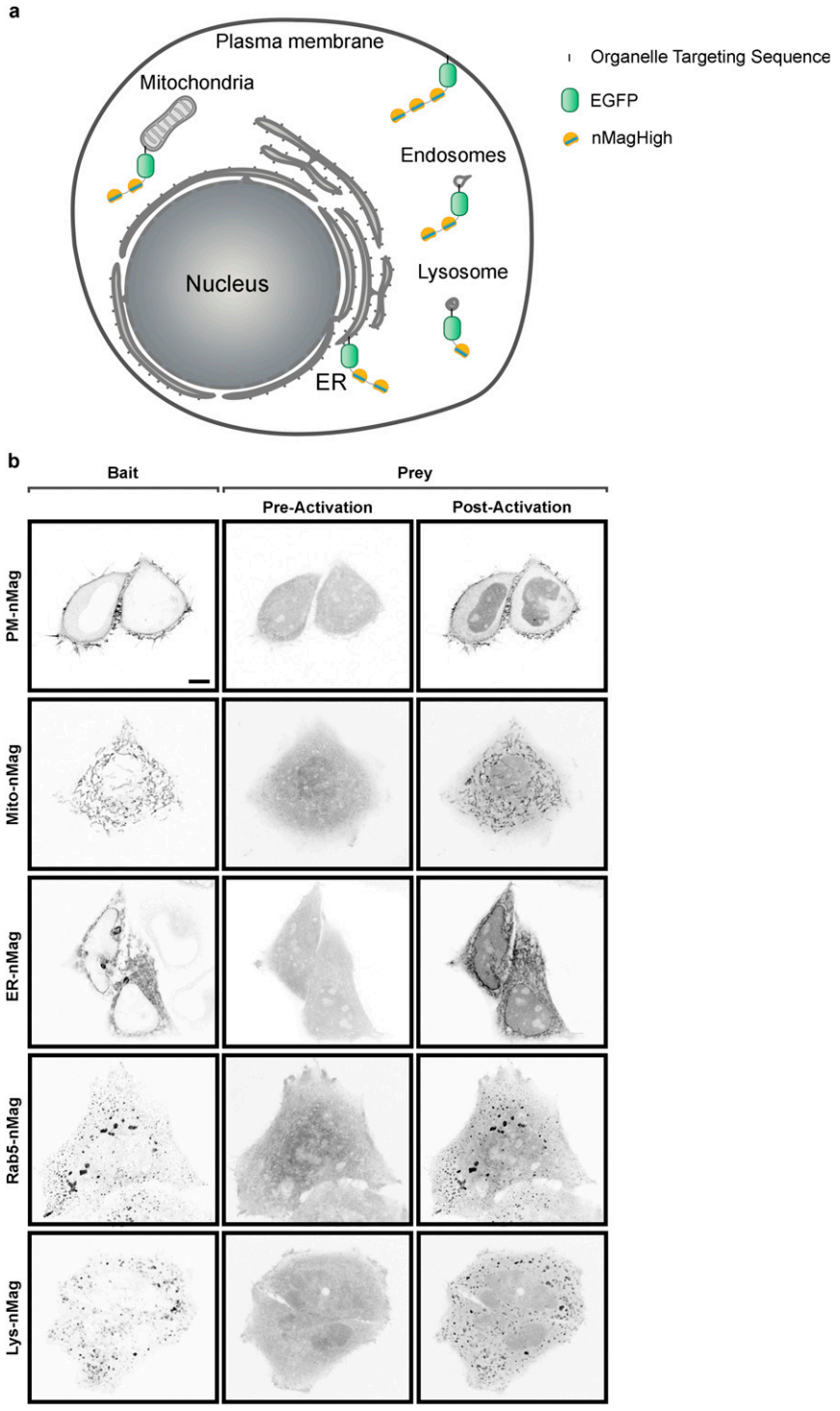

Fig. S4. Magnet baits targeting different subcellular compartments. (*A*) Illustration depicting the molecular composition and localization of each organelle-specific bait generated. Each bait is composed of an organelle-targeting sequence (OTS) fused to EGFP and a given number of nMagHigh1 molecules interconnected by proper linker regions (see Table S1 for full constructs details). (*B*) Efficient targeting of a soluble prey [pMagFast2(3x)-mCherry] to bait localized on different subcellular organelles in HeLa cells: plasma membrane-specific bait (PM-nMag), mitochondria-specific bait (Mito-nMag), endoplasmic reticulum-specific bait (ER-nMag), early endosome-specific bait (Rab5-nMag), and lysosome-specific bait (Lyso-nMag). (Scale bar: 5 μm.)

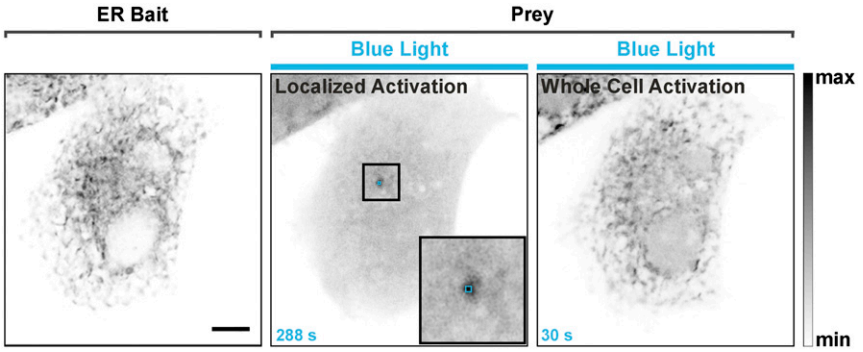

Fig. S5. Control of protein dimerization in a very small portion, 1 μm^2 (x–y dimension), of the ER by Magnets. HeLa cell expressing ER-nMag (bait) and pMagFast2(3x)-tgRFPt (prey) upon localized or whole-cell illumination. The blue square indicates the area of light delivery. (Magnification: *Center Insets*, 5×.) (Scale bar: 10 μm.)

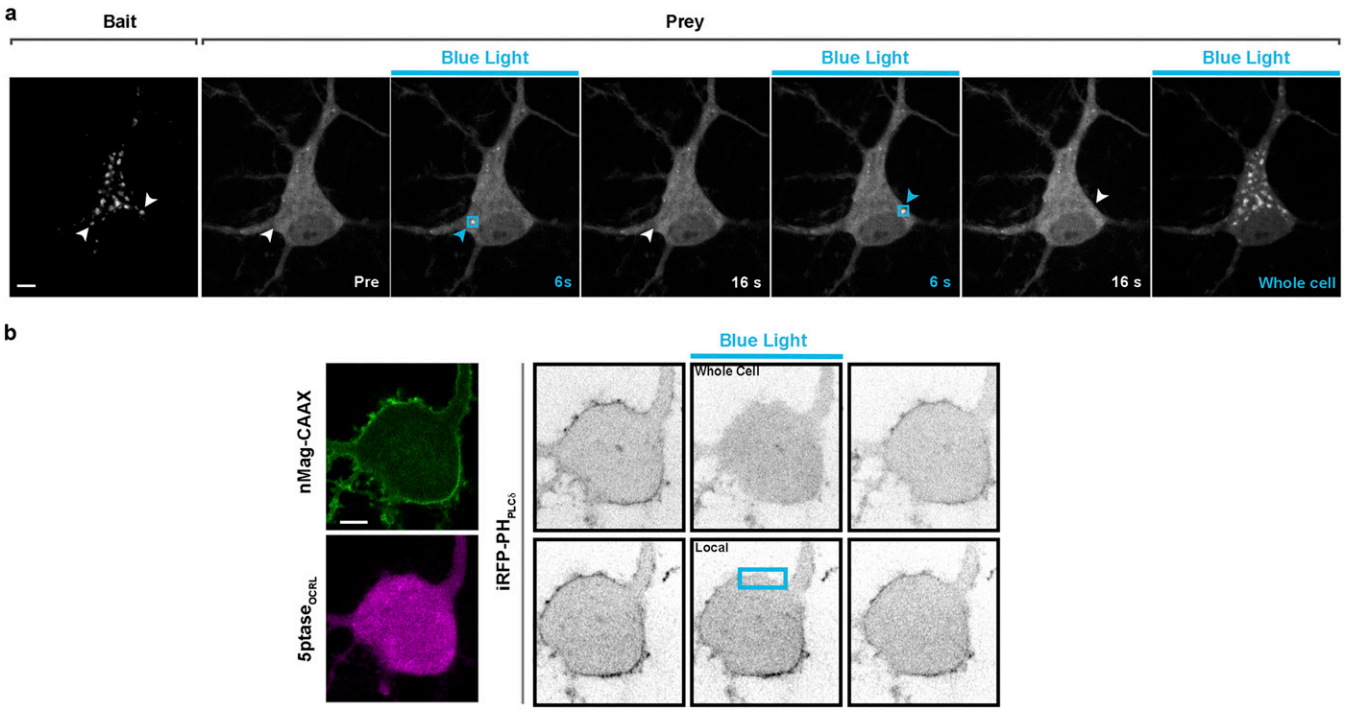

Fig. S6. Optical control of protein dimerization on a single organelle and on a portion of the plasma membrane in primary neurons. (*A*) Primary cortical neuron (7 DIV) expressing a lysosomal bait (Lys-nMag), a soluble prey [pMagFast2(3x)-tgRFPt], and a specific marker for lysosomes (iRFP-Lamp1). The series of micrographs shows reversible prey protein recruitment to single lysosomes (arrows) or to the entire lysosomal population (whole-cell illumination shown at the right) in a blue-light-dependent and reversible way. (Scale bar: 5 μm.) (*B*) Reversible and light-dependent depletion of $PI(4,5)P_2$ at the plasma membrane in primary hippocampal neurons (12 DIV), as detected by the $PI(4,5)P_2$ reporter iRFP-$PH_{PLC\delta}$. The effects of whole-cell and focal illumination are shown. (Scale bar: 5 μm.)

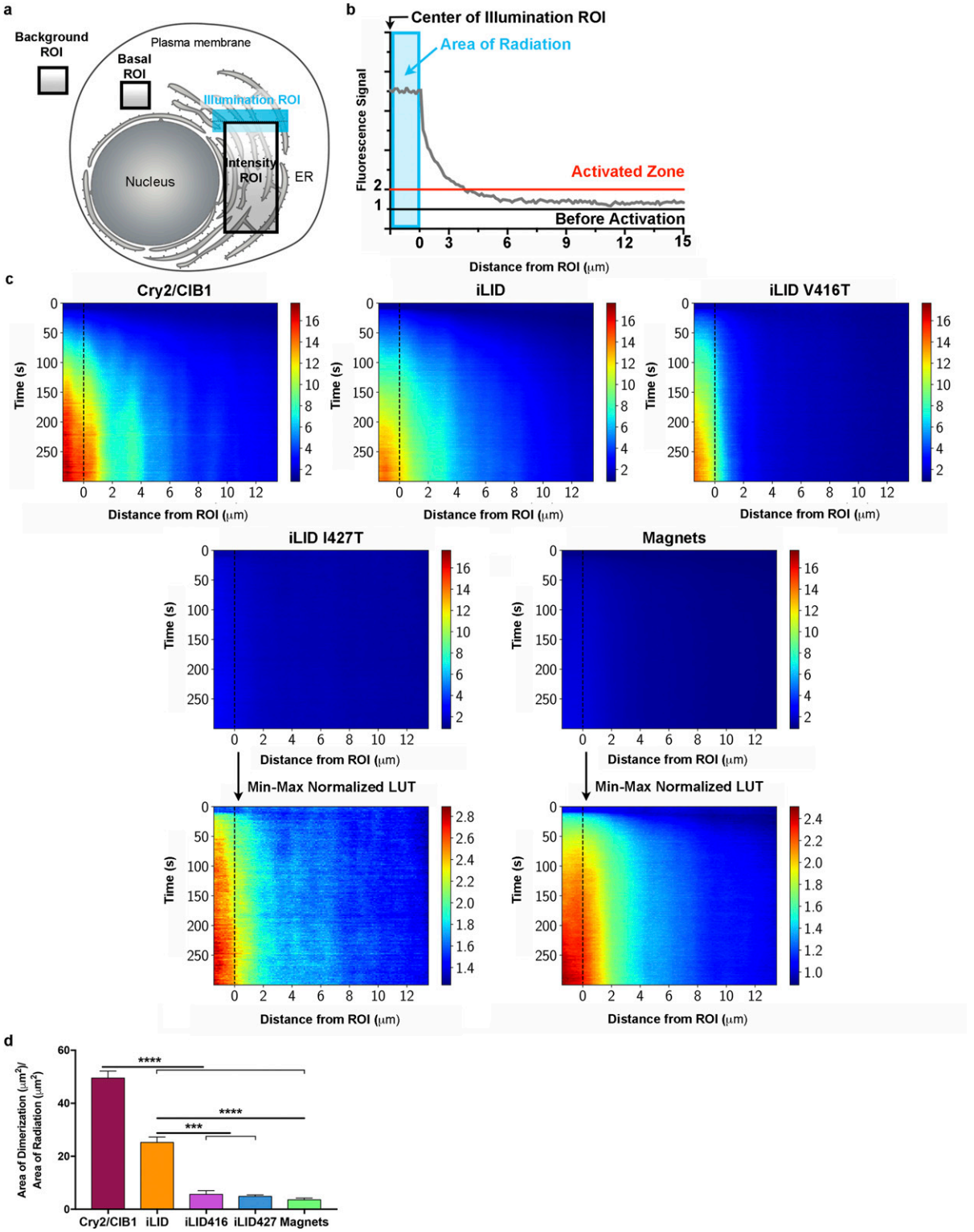

Fig. S7. Magnets enable a higher spatial confinement of protein dimerization to the area of photoexcitation. (*A*) Cell schematic showing the Intensity ROI (black rectangle) created to measure the extent of protein dimerization outside of the photoexcitation area (blue rectangle). (*B*) We defined the spread distance from the area of radiation as the farthest positive distance from the edge of the Illumination ROI (blue area) at which the fluorescence intensity increases by 100% over that of the Basal ROI (area denoted by activated zone, Basal ROI shown in *A*). (*C*) Heat maps showing the spatial extent of dimerization for each system. The normalized intensity (*SI Materials and Methods*) is represented with the color of each pixel ($n = 12$ for Cry2/CIB1, 13 for iLID, 10 for iLID V416T, 6 for iLID I427T, and 17 cells for Magnets; $n = 3$). (*D*) Histogram showing the ratio between the dimer-positive area and the area of blue-light radiation after 5 min of photoexcitation. The area of dimer formation for Cry2/CIB1 is 49.1 ± 2.7 times the radiation area ($n = 30$; $n = 3$), for iLID is 25.2 ± 2.1 times ($n = 26$; $n = 3$), for iLID V416T is 5.6 ± 1.4 times ($n = 14$; $n = 3$), for iLID I427T is 4.9 ± 0.6 times ($n = 14$; $n = 3$), and for Magnets is 3.6 ± 0.6 times the radiation area ($n = 24$; $n = 3$). Data were evaluated with one-way ANOVA followed by Tukey's multiple comparison test, with the software GraphPad Prism. ****$P < 0.0001$, ***$P < 0.001$.

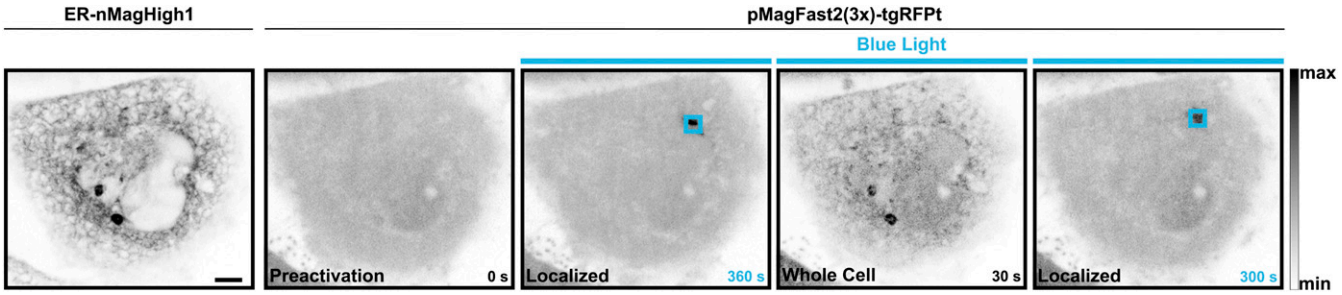

Fig. S8. Local protein dimerization with Magnets does not change before and after whole-cell activation. HeLa cell cotransfected with the ER bait ER-nMag and the soluble prey pMagFast2(3x)-tgRFPt. Prolonged pulsed illumination (360 s) of the soluble pMagFast2(3x)-tgRFPT fusion protein in a 3-μm × 3-μm area (blue box) results in the progressive accumulation of the probe in the area of radiation. Upon irradiation of the whole field of view the protein is recruited to ER and nMagHigh1 is activated for hours in the whole intracellular compartment. If localized excitation in a 3-μm × 3-μm area (blue box) is redelivered to the sample after 1 min of recovery the soluble pMagFast2(3x)-tgRFPt fusion protein is still accumulated in a very restricted portion of the ER. (Scale bar: 5 μm.)

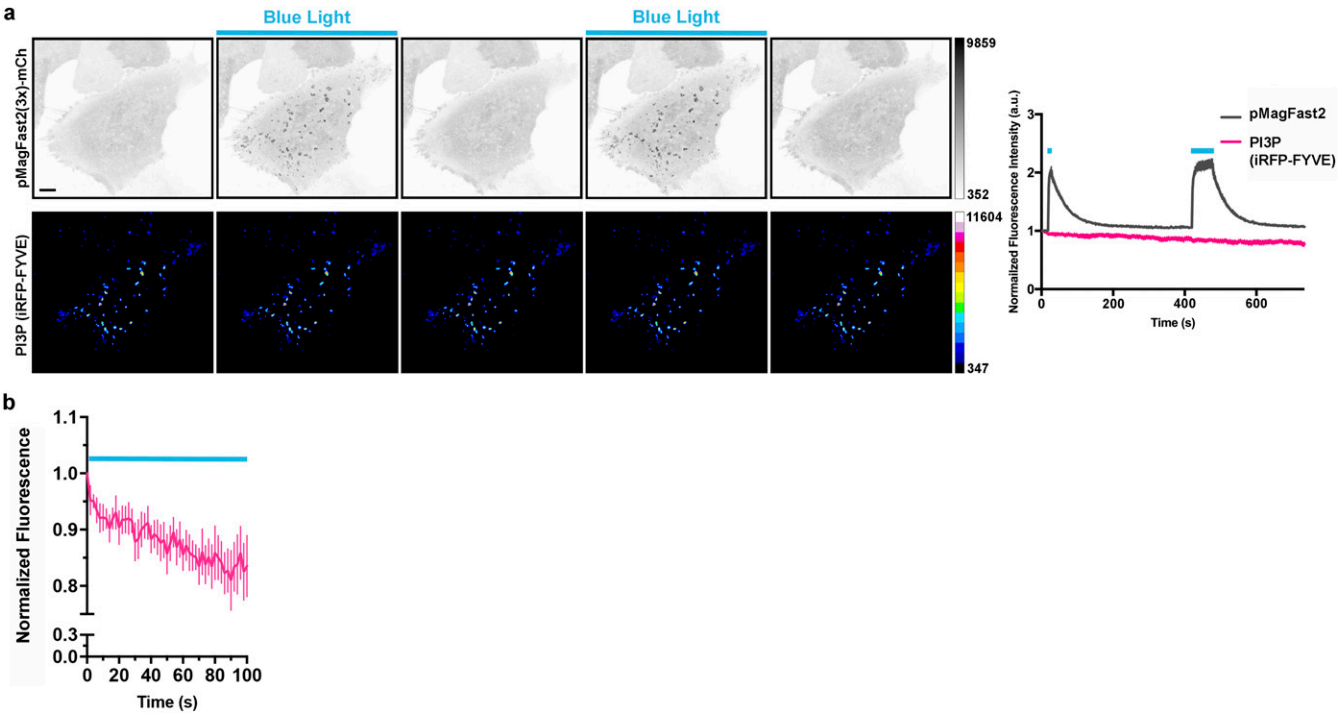

Fig. S9. The endosomal recruitment of pMagFast2(3x)-mCherry does not affect PI3P levels if it is not fused to MTMR1. (*A*) HeLa cell expressing Rab5-nMag (not shown), pMagFast2(3x)-mCherry (inverted gray scale), and the PI3P reporter iRFP-FYVE (16-colors scale). Whole-cell illumination induces a light-dependent and completely reversible recruitment of pMagFast2(3x)-mCherry to Rab5 endosomes. This recruitment does not cause any change in endosomal PI3P levels. Changes in fluorescence were measured in 31 endosomes while inducing prey association to endosomes with two blue-light pulses of different duration. (Scale bar: 10 μm.) (*B*) The recruitment of MTMR1 to endosomes upon whole-cell illumination induces a reduction of the PI3P reporter iRFP-FYVE of 20% ($n = 10$ cells; $n = 3$).

Table S1. Magnets baits targeting differential subcellular compartments

Name	Localization	OTS position	Origin	NCBI accession no.	Fused amino acid sequence	No. of nMagHigh repeats	Fluorescent tag
PM-nMag(1x)	Plasma membrane	C-ter	Isoform 2B of GTPase KRas (*H. sapiens*)	P01116-2	KKKKKKSKTKCVIM	1	EGFP
PM-nMag(3x)	Plasma membrane	C-ter	Isoform 2B of GTPase KRas (*H. sapiens*)	P01116-2	KKKKKKSKTKCVIM	3	EGFP
Mito-nMag(1x)	Mitochondria	C-ter	Outer membrane protein OMP25 or synaptojanin-2-binding protein (*H. sapiens*)	NP_060843.2	VQNGPIGHRGEGDPSGIPIFMVLVPVFALTMVA-AWAFMRYRQQL	1	EGFP
Mito-nMag(2x)	Mitochondria	C-ter	Outer membrane protein OMP25 or synaptojanin-2-binding protein (*H. sapiens*)	NP_060843.2	VQNGPIGHRGEGDPSGIPIFMVLVPVFALTMVA-AWAFMRYRQQL	2	EGFP
ER-nMag	ER	N-ter	Cytochrome P450 2C1 (*Oryctolagus cuniculus*)	AAA31436	MDPVVVLGLCLSCLLLLSLWKQSYGGG	2	EGFP
Lys-nMag	Lysosomes	N-ter	Ragulator complex protein LAMTOR1 (*H. sapiens*)	NP_060377.1	MGCCYSSENEDSDQDREERKLLLDPSSPPTKAL-NGAEPNY	1	EGFP
Rab5-nMag	Early endosomes	C-ter	Rab5A (*Canis lupus familiaris*)	M35520.1	MANRGATRPNGPNTGNKICQFKLVLLGESAVG-KSS LVLRFVKGQFHEFQESTIGAAFLTQTVCL-DDTTVKFEIWDTAGQERYHSLAPMYYRGAQ-AAIVVYDITNEESFARAKNWVKELQRQASPN-IVIALSGNKADLANKRAVDFQEAQSYADDNS-LLFMETSAKTSMNVNEIFMAIAKKLPKNEPQN-PGANSARGRGVDLTEPTQPTRSQCCSN	2	EGFP

OTS used, position, and nMagHigh units used for each subcellular compartment are shown.

Table S2. Baits targeting differential subcellular compartments for iLID and Cry2/CIB1 systems

Name	Localization	OTS position	Origin	NCBI accession no.	Fused amino acid sequence	No. of dimerizer units	Fluorescent tag
ER-iLID	ER	N-ter	Cytochrome P450 2C1 (*O. cuniculus*)	AAA31436	MDPVVVLGLCLSCLLLLSLWKQSYGGG	1	mVenus
ER-CIBN	ER	N-ter	Cytochrome P450 2C1 (*O. cuniculus*)	AAA31436	MDPVVVLGLCLSCLLLLSLWKQSYGGG	1	EGFP
iLID-Mito	Mitochondria	C-ter	pLL7.0: Venus-iLID-Mito (From ActA) was a gift from Brian Kuhlman, University of North Carolina at Chapel Hill, Chapel Hill, NC (Addgene plasmid 60,413) (*Listeria monocytogenes*)	CP019623.1	LIAKSAEDEKAKEEPGNHTTLILAMLAI-GVFSLGAFIKIIQLRKNN	1	mVenus
CIBN-Mito	Mitochondria	C-ter	Outer membrane protein OMP25 or synaptojanin-2-binding protein (*H. sapiens*)	NP_060843.2	VQNGPIGHRGEGDPSGIPIFMVLVPVFA-LTMVAAWAFMRYRQQL	2	EGFP

OTS and position used for each subcellular compartment are shown.

Table S3. Switch-on and -off kinetics calculated for each dimerization pair

Dimerization pair	$\tau_{1/2}^{ON}$, s	$\tau_{1/2}^{OFF}$, s
CRY2PHR-CIBN	3.7 ± 0.9	290 ± 30
iLID–SspB wt	2.0 ± 0.3	28 ± 1
iLID–SspB R73Q	1.5 ± 0.2	34 ± 5
iLID V416T–SspB R73Q	2.7 ± 0.3	5 ± 5
iLID I427T–SspB R73Q	1.2 ± 0.3	4 ± 1
nMagHigh1(1x)–pMagFast2(3x)	1.2 ± 0.2	3 ± 2
nMagHigh1(2x)–pMagFast2(3x)	1.4 ± 0.1	15 ± 3

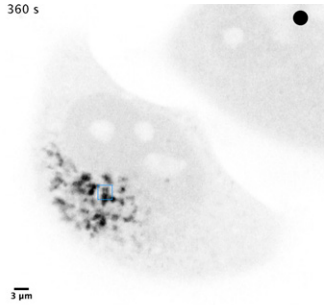

Movie S1. Locally activated Cry2 can diffuse and bind to ER-bound bait throughout the cell. HeLa cell expressing ER-CIBN and mCherry-Cry2. Despite the local irradiation of a 3-µm × 3-µm region (blue square) with 488-nm light pulses of 200 ms every 2 s, activated Cry2 diffuses outside of the activation area and binds to its interacting partner expressed on the surface of the ER away from the illuminated area. (Scale bar: 3 µm.)

Movie S1

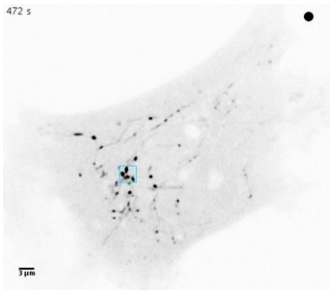

Movie S2. Locally activated Cry2 can diffuse and bind to mitochondrial bait throughout the cell. Human fibroblast expressing CIBN-Mito and mCherry-Cry2. Despite the local radiation with 488-nm light pulses of 200 ms every 2 s in a 3-µm × 3-µm region (blue square), the activated photoreceptor diffuses outside of the activation area and, in a few minutes, a substantial amount of Cry2 is detectable on the mitochondria away from the illuminated area. (Scale bar: 3 µm.)

Movie S2

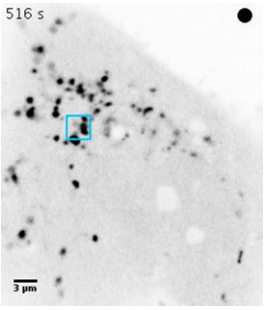

Movie S3. Homooligomerization of activated Cry2 is enhanced when concentrated on the surface of an organelle. Human fibroblast expressing CIBN-Mito and mCherry-Cry2. The Cry2/CIB1 system was activated by 488-nm laser pulses delivered to a 3-μm × 3-μm area (blue square), as indicated. The enrichment of activated Cry2 on the surface of an organelle (mitochondria in this case) dramatically facilitates homooligomerization of activated Cry2. (Scale bar: 3 μm.)

Movie S3

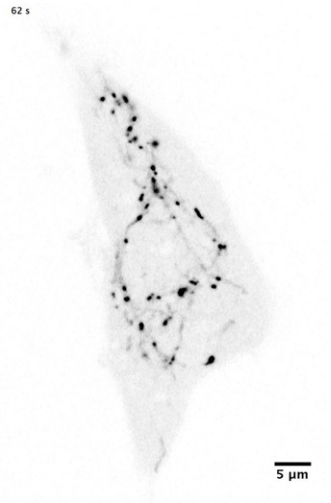

Movie S4. Activated Cry2 homooligomerization on the surface of small organelles under whole-cell irradiation. Human fibroblast expressing CIBN-Mito and mCherry-Cry2. The Cry2/CIB1 system was activated throughout the cell by a single 488-nm laser pulse of 200 ms. Cry2 homooligomerization process only starts after accumulation of activated Cry2 on the surface of mitochondria. (Scale bar: 5 μm.)

Movie S4

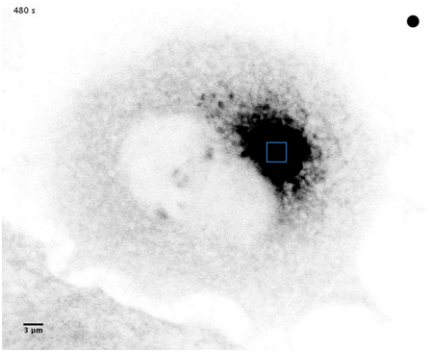

Movie S5. Spatial control of protein recruitment on the ER with iLID. HeLa cell expressing ER-iLID and tgRFPt-SspB Micro. Blue-light pulses of 200 ms were delivered to a 3-µm × 3-µm region every 2 s for 5 min. Although the photoreceptor is associated to the ER membrane, and thus activated only in the irradiated area of the ER, dimer presence, as reflected by prey accumulation, rapidly spreads over a broader area of the ER. (Scale bar: 3 µm.)

Movie S5

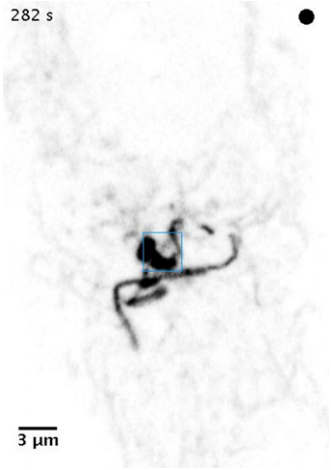

Movie S6. Spatial control of protein interaction at mitochondria with iLID. Human fibroblast expressing iLID-Mito and mCherry-SspB Micro. Despite the local radiation in 3 µm × 3 µm with 488-nm light pulses of 200 ms every 2 s, dimer presence, as reflected by prey accumulation, rapidly spreads over a broader area of the mitochondrial network. Additionally, the high binding affinity of SspB Micro for iLID is responsible for a nonnegligible interaction of the two proteins, and thus nonnegligible presence of the prey on mitochondria, in the inactive state. (Scale bar: 3 µm.)

Movie S6

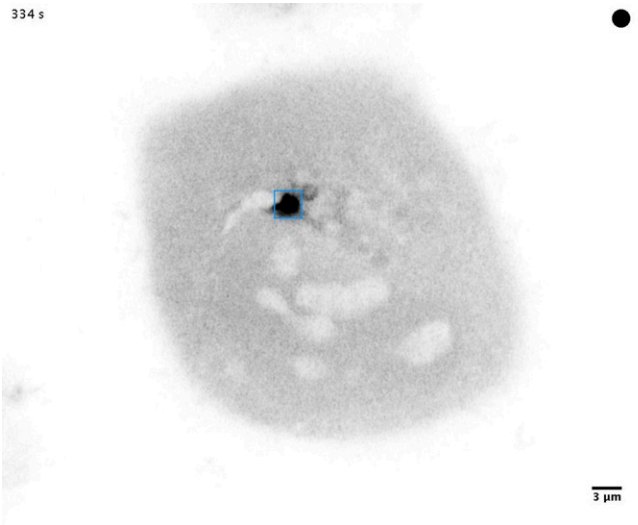

Movie S7. High spatial confinement of optical dimerization on the ER achieved by Magnets. HeLa cell expressing ER-nMag and pMagFast2(3x)-tgRFPt. Blue-light pulses of 200 ms were delivered to a 3-µm × 3-µm region every 2 s for 5 min. The dimerization of the two photoswitches is spatially confined to the photoexcitation area of the ER. (Scale bar: 3 µm.)

Movie S7

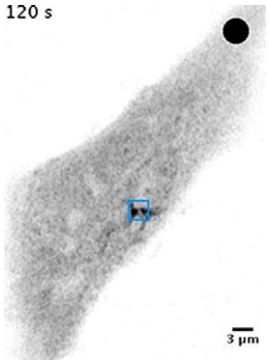

Movie S8. High spatial confinement of optical dimerization on the mitochondrial network achieved by Magnets. Human fibroblast expressing Mito-nMag(2x) and pMagFast2(3x)-mCherry. Dimer is predominantly confined to the area of photoactivation. (Scale bar: 3 µm.)

Movie S8

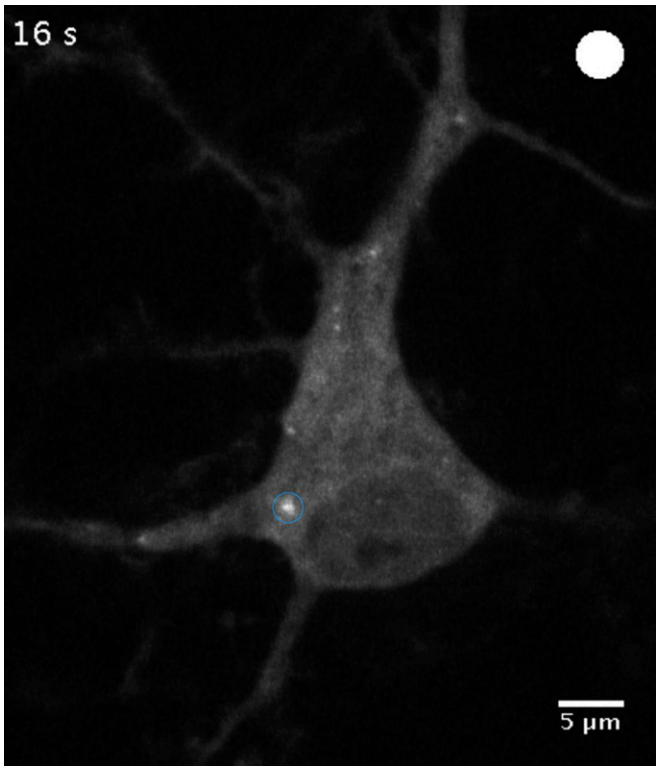

Movie S9. Light-dependent protein recruitment to a single lysosome in primary neurons. Primary cortical neuron (7 DIV) expressing a lysosomal bait (Lys-nMag), a soluble prey [pMagFast2(3x)-tgRFPt], and a specific marker of lysosomes (iRFP-Lamp1). The blue circle indicates the area of blue-light radiation. The white dot on the right corner indicates presence of illumination. (Scale bar: 5 µm.)

Movie S9

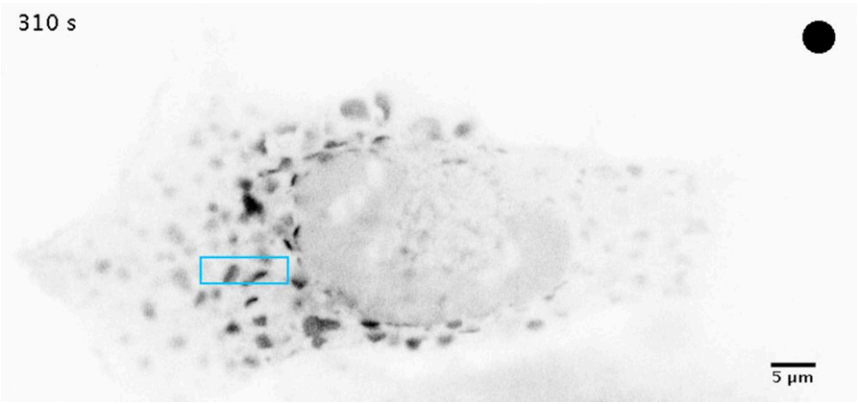

Movie S10. Progressive spread to entire cell of the presence of the Cry2/CIB1 dimer at the ER surface upon prolonged illumination. HeLa cell expressing ER-CIBN and mCherry-Cry2. Despite the local irradiation of a 3-µm × 10-µm region with 488-nm light pulses of 200 ms every 2 s the activated Cry2 freely diffuses outside of the photoactivation area and binds its interacting partner expressed on the surface of the ER throughout the cell. (Scale bar: 3 µm.)

Movie S10

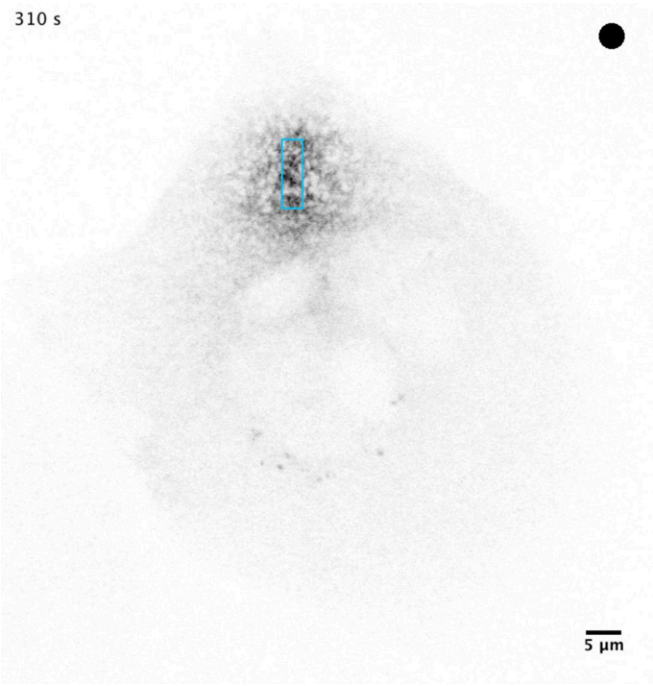

Movie S11. Limited spread of the dimer at the surface of the ER with the iLID system. HeLa cell expressing ER-iLID and tgRFPt-SspB Micro. Blue-light pulses of 200 ms were delivered in a region of 3 μm × 10 μm every 2 s for 5 min. Bait–prey dimer is limited to a portion of the ER but not restricted to the area of photoexcitation. (Scale bar: 3 μm.)

Movie S11

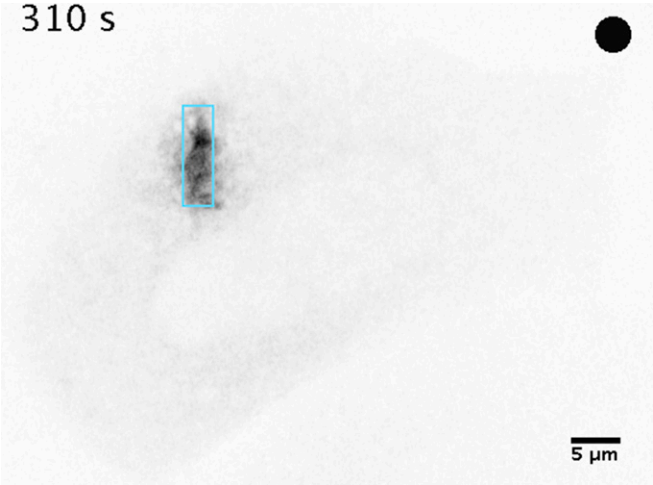

Movie S12. The use of iLID V416T enables a higher degree of spatial confinement of dimer formation at the ER. HeLa cell expressing ER-iLID V416T and tgRFPt-SspB Micro. Blue-light pulses of 200 ms were delivered in a region of 3 μm × 10 μm every 2 s for 5 min. The confinement of the bait–prey dimer on the ER achieved by this iLID is greater than the one achieved by the iLID pair with a longer switch-off kinetic but it is still not restricted to the area of photoexcitation. (Scale bar: 3 μm.)

Movie S12

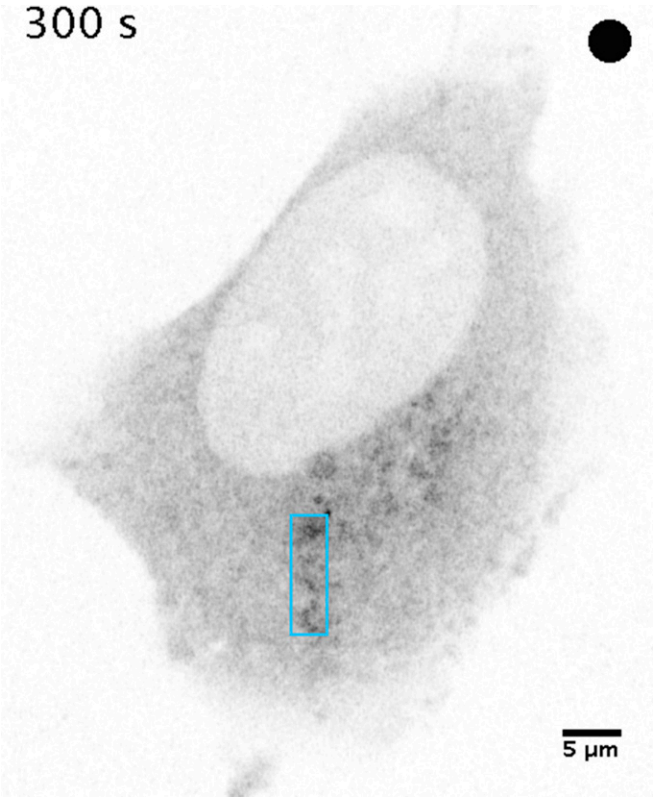

Movie S13. The use of iLID I427T enables a higher degree of spatial confinement of dimer formation at the ER. HeLa cell expressing ER-iLID I427T and tgRFPt-SspB Micro. Blue-light pulses of 200 ms were delivered in a region of 3 µm × 10 µm every 2 s for 5 min. The confinement of the bait–prey dimer on the ER achieved by this iLID is greater than the one achieved by the iLID pair with a longer switch-off kinetic but it is still not restricted to the area of photoexcitation. (Scale bar: 3 µm.)

Movie S13

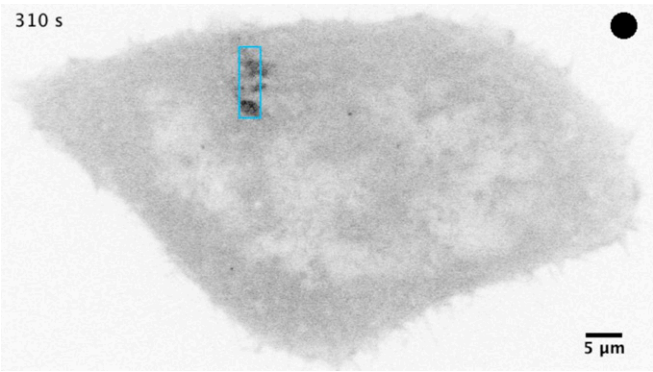

Movie S14. The Magnets system limits bait–prey interaction to the area of light radiation. HeLa cell expressing ER-nMag and pMagFast2(3x)-tgRFPt. Blue-light pulses of 200 ms were delivered in a region of 3 µm × 10 µm every 2 s for 5 min. The dimerization of the two photoswitches is spatially confined to the photoexcitation area throughout the photostimulation period. (Scale bar: 3 µm.)

Movie S14

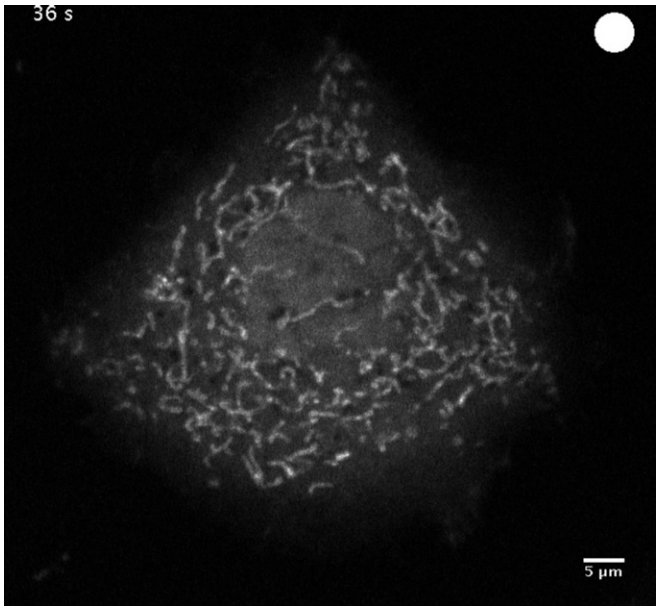

Movie S15. Optically dependent knocksideways of a cytosolic protein using Magnets. HeLa cell expressing Mito-nMag(2x) and pMagFast2(3x)-mCherry. Rapid, light-dependent, and reversible depletion of a cytosolic protein by recruiting it to mitochondria. (Scale bar: 10 µm.)

Movie S15

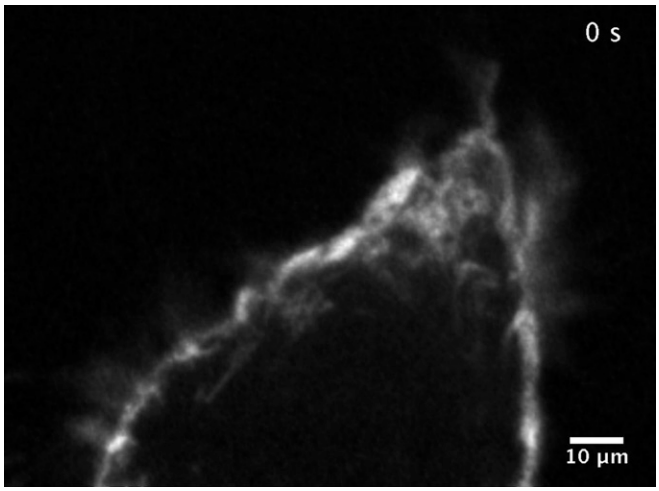

Movie S16. Reversible dephosphorylation of PI(4,5)P_2 at the plasma membrane using Magnets. HeLa cell expressing PM-nMagHigh1(3x), mCherry-pMagFast2(3x)-5ptase$_{OCRL}$, and iRFP-PH-PLC$_{delta}$ (PI(4,5)P_2 reporter). Cell stimulation with blue-light pulses induces the rapid association and dissociation of the 5ptase domain of OCRL at the plasma membrane and the concomitant reduction of PI(4,5)P_2 levels. This causes the dissociation and association, respectively, of the PI(4,5)P_2 reporter (iRFP-PH$_{PLCdelta}$)(channel shown). The white dot indicates presence of illumination. (Scale bar: 10 µm.)

Movie S16

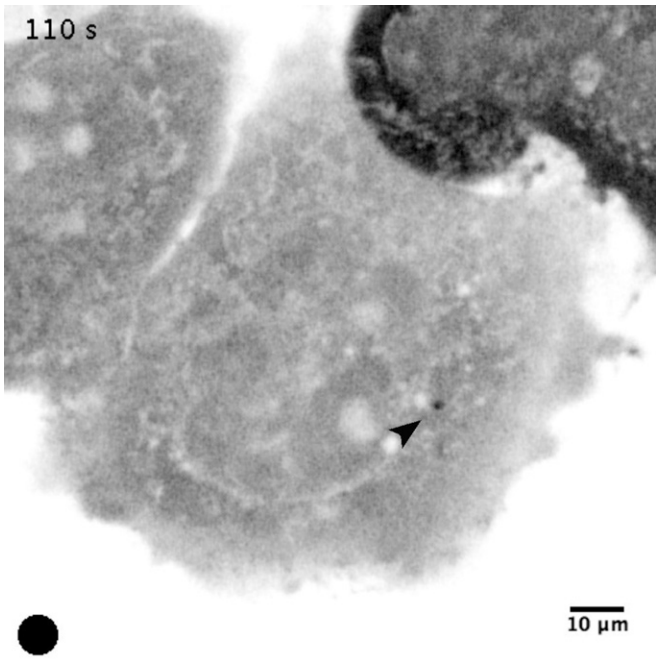

Movie S17. Light-induced recruitment of a prey to a single lysosome using Magnets. HeLa cell expressing Lys-nMag, pMagFast2(3x)-tgRFPt, and iRFP-Lamp1. Lamp1 fluorescence signal allows the visualization of lysosomes (signal not shown). The localized radiation of a selected lysosome (arrow head) induces the recruitment of the soluble prey to a single organelle in a light-dependent and reversible way. The black dot indicates presence of illumination. (Scale bar: 10 µm.)

Movie S17

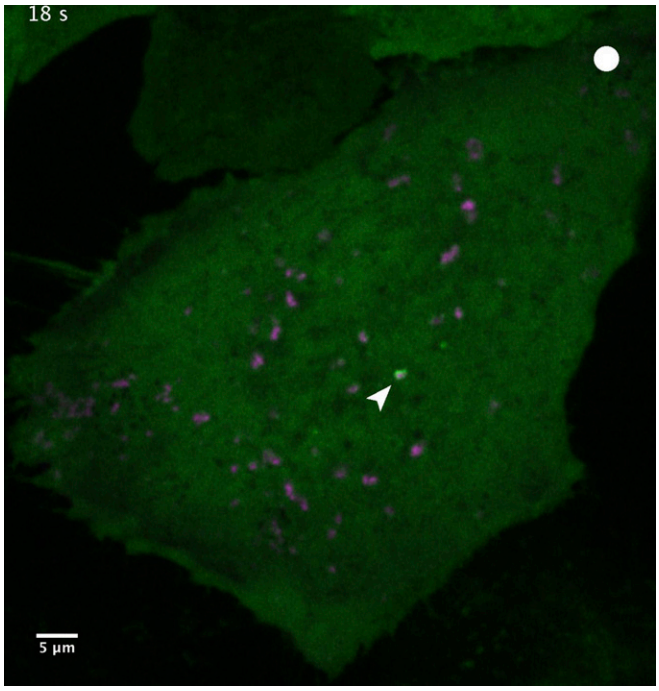

Movie S18. Light-induced protein recruitment of a prey to single endosomes using Magnets. HeLa cell expressing nMag-Rab5, pMagFast2(3x)-tgRFPt, and iRFP-FYVE (PI3P reporter). iRFP-FYVE fluorescence signal (channel in magenta) was used to identify early endosomes. The localized radiation of a selected endosome (arrow head) allows recruitment of the soluble prey (green channel) in a light-dependent and reversible way. The white dot indicates presence of illumination. (Scale bar: 5 µm.)

Movie S18